Sensitivities of InGaAsP photonic crystal membrane nanocavities to hole refractive index

Sensitivities of InGaAsP photonic crystal membrane nanocavities to hole refractive index

Mehmet A. Dündar,[1,2,*] Els C. I. Ryckebosch,[1,2] Richard Nötzel,[1,2] Fouad Karouta,[1] Leo J. van IJzendoorn,[2] and Rob W. van der Heijden[1,2]

[1]*COBRA Research Institute, Eindhoven University of Technology, P.O. Box 513, NL-5600MB Eindhoven, The Netherlands*

[2]*Department of Applied Physics, Eindhoven University of Technology, P.O. Box 513, NL-5600MB Eindhoven, The Netherlands*

**m.dundar@tue.nl*

Abstract: The sensitivities of resonant wavelengths of photonic crystal (PhC) membrane nanocavities with embedded InAs quantum dots to the ambient refractive index are reported for use in (bio) chemical sensing. The resonances for the different modes of several point-defect type cavities are obtained by photoluminescence measurements. Systematic trends of the variation of sensitivity with increase of the overlap of the modes with the PhC holes are observed for varying cavity type as well as for a given mode within a cavity type. A maximum sensitivity of ~300 nm/RIU (refractive index unit) is observed, corresponding to ~25% mode overlap with the holes and complete infiltration with the aqueous solution.

OCIS codes: (230.5298) Photonic crystals; (230.5750) Resonators; (280.4788) Optical sensing and sensors.

References and links

1. B. Liedberg, I. Lundstrom, and E. Stenberg, "Principles of biosensing with an extended coupling matrix and surface-Plasmon resonance," Sens. Actuators B Chem. **11**(1-3), 63–72 (1993).
2. B. J. Luff, J. S. Wilkinson, J. Piehler, U. Hollenbach, J. Ingenhoff, and N. Fabricius, "Integrated optical Mach-Zehnder biosensor," J. Lightwave Technol. **16**(4), 583–592 (1998).
3. R. G. Heideman, and P. V. Lambeck, "Remote opto-chemical sensing with extreme sensitivity: design, fabrication, and performance of a pigtailed intergrated optical phase-modulated Mach-Zehnder interferometer system," Sens. Actuators B Chem. **61**(1-3), 100–127 (1999).
4. V. Mulloni, and L. Pavesi, "Porous silicon microcavities as optical chemical sensors," Appl. Phys. Lett. **76**(18), 2523–2525 (2000).
5. K. J. Vahala, "Optical microcavities," Nature **424**(6950), 839–846 (2003).
6. A. Yalcin, K. C. Popat, J. C. Aldridge, T. A. Desai, J. Hryniewicz, N. Chbouki, B. E. Little, O. King, V. Van, S. Chu, D. Gill, M. Anthes-Washburn, and M. S. Unlu, "Optical sensing of biomolecules using microring resonators," IEEE J. Sel. Top. Quantum Electron. **12**(1), 148–155 (2006).
7. C. Monat, P. Domachuk, and B. J. Eggleton, "Integrated optofluidics: A new river of light," Nat. Photonics **1**(2), 106–114 (2007).
8. N. Jokerst, M. Royal, S. Palit, L. Luan, S. Dhar, and T. Tyler, "Chip scale integrated microresonator sensing systems," J. Biophoton. **2**(4), 212–226 (2009).
9. J. B. Jensen, L. H. Pedersen, P. E. Hoiby, L. B. Nielsen, T. P. Hansen, J. R. Folkenberg, J. Riishede, D. Noordegraaf, K. Nielsen, A. Carlsen, and A. Bjarklev, "Photonic crystal fiber based evanescent-wave sensor for detection of biomolecules in aqueous solutions," Opt. Lett. **29**(17), 1974–1976 (2004).
10. K. De Vos, I. Bartolozzi, E. Schacht, P. Bienstman, and R. Baets, "Silicon-on-Insulator microring resonator for sensitive and label-free biosensing," Opt. Express **15**(12), 7610–7615 (2007).
11. M. Lončar, A. Scherer, and Y. M. Qiu, "Photonic crystal laser sources for chemical detection," Appl. Phys. Lett. **82**(26), 4648–4650 (2003).
12. E. Chow, A. Grot, L. W. Mirkarimi, M. Sigalas, and G. Girolami, "Ultracompact biochemical sensor built with two-dimensional photonic crystal microcavity," Opt. Lett. **29**(10), 1093–1095 (2004).
13. M. R. Lee, and P. M. Fauchet, "Two-dimensional silicon photonic crystal based biosensing platform for protein detection," Opt. Express **15**(8), 4530–4535 (2007).
14. D. F. Dorfner, T. Hurlimann, T. Zabel, L. H. Frandsen, G. Abstreiter, and J. J. Finley, "Silicon photonic crystal nanostructures for refractive index sensing," Appl. Phys. Lett. **93**(18), 181103 (2008).

#122028 - $15.00 USD Received 4 Jan 2010; revised 1 Feb 2010; accepted 1 Feb 2010; published 16 Feb 2010

15. S. Kita, K. Nozaki, and T. Baba, "Refractive index sensing utilizing a cw photonic crystal nanolaser and its array configuration," Opt. Express **16**(11), 8174–8180 (2008).
16. S. Mandal, and D. Erickson, "Nanoscale optofluidic sensor arrays," Opt. Express **16**(3), 1623–1631 (2008).
17. S. Kim, J. Lee, H. Jeon, and H. J. Kim, "Fiber-coupled surface-emitting photonic crystal band edge laser for biochemical sensor applications," Appl. Phys. Lett. **94**(13), 133503 (2009).
18. M. Loncar, "Molecular sensors: Cavities lead the way," Nat. Photonics **1**(10), 565–567 (2007).
19. A. Di Falco, L. O'Faolain, and T. F. Krauss, "Chemical sensing in slotted photonic crystal heterostructure cavities," Appl. Phys. Lett. **94**(6), 063503 (2009).
20. R. Nötzel, S. Anantathanasarn, R. P. J. van Veldhoven, F. W. M. van Otten, T. J. Eijkemans, A. Trampert, B. Satpati, Y. Barbarin, E. A. J. M. Bente, Y. S. Oei, T. de Vries, E. J. Geluk, B. Smalbrugge, M. K. Smit, and J. H. Wolter, "Self Assembled InAs/InP Quantum Dots for Telecom Applications in the 1.55 μm Wavelength Range: Wavelength Tuning, Stacking, Polarization Control, and Lasing," Jpn. J. Appl. Phys. **45**(No. 8B), 6544–6549 (2006).
21. H. G. Park, J. K. Hwang, J. Huh, H. Y. Ryu, S. H. Kim, J. S. Kim, and Y. H. Lee, "Characteristics of modified single-defect two-dimensional photonic crystal lasers," IEEE J. Quantum Electron. **38**(10), 1353–1365 (2002).
22. F. Intonti, S. Vignolini, V. Turck, M. Colocci, P. Bettotti, L. Pavesi, S. L. Schweizer, R. Wehrspohn, and D. Wiersma, "Rewritable photonic circuits," Appl. Phys. Lett. **89**(21), 211117 (2006).
23. C. L. C. Smith, D. K. C. Wu, M. W. Lee, C. Monat, S. Tomljenovic-Hanic, C. Grillet, B. J. Eggleton, D. Freeman, Y. Ruan, S. Madden, B. Luther-Davies, H. Giessen, and Y. H. Lee, "Microfluidic photonic crystal double heterostructures," Appl. Phys. Lett. **91**(12), 121103 (2007).
24. F. Intonti, S. Vignolini, F. Riboli, M. Zani, D. S. Wiersma, L. Balet, L. H. H. Li, M. Francardi, A. Gerardino, A. Fiore, and M. Gurioli, "Tuning of photonic crystal cavities by controlled removal of locally infiltrated water," Appl. Phys. Lett. **95**(17), 173112 (2009).
25. F. Schneider, ed., *Sugar Analysis-ICUMSA*, (International Commission for Uniform Methods of Sugar Analysis, (ICUMSA), 1979, (ICUMSA), 2009).
26. S. Tomljenovic-Hanic, A. Rahmani, M. J. Steel, and C. M. de Sterke, "Comparison of the sensitivity of air and dielectric modes in photonic crystal slab sensors," Opt. Express **17**(17), 14552–14557 (2009).
27. I. M. White, and X. D. Fan, "On the performance quantification of resonant refractive index sensors," Opt. Express **16**(2), 1020–1028 (2008).
28. S. H. Kim, J. H. Choi, S. K. Lee, S. H. Kim, S. M. Yang, Y. H. Lee, C. Seassal, P. Regrency, and P. Viktorovitch, "Optofluidic integration of a photonic crystal nanolaser," Opt. Express **16**(9), 6515–6527 (2008).

1. Introduction

Photonics-based devices are very attractive for (bio) chemical sensing since they are easily incorporated in fluid cells containing the analyte. The surface of light guiding structures can be functionalized with target-specific binding layers. The sensing is based on the change in refractive index experienced by the electromagnetic field near the surface with the presence of the target molecules, so that the target does not require any fluorescent labeling. Label-free sensors are important, not only because they avoid expensive and laborious labeling steps, but also because the labels may affect the biochemical recognition. So far, various label-free (bio) chemical sensors have been demonstrated, capable of measuring the refractive index change of the environment with high resolution [1–7]. The most developed sensors are the Surface Plasmon Resonance [1] and Mach-Zehnder interferometer [2,3] based devices, that require a large sensing area (~mm^2) which is one of the main limitations for integrating these sensors in optical chips.

Miniaturization of label-free optical sensors is of particular interest for realizing ultra compact lab-on-a-chip applications with dense arrays of functionalized spots for multiplexed sensing, that may lead to portable, low cost and low power devices [8]. Many efforts exist to realize small devices and among them are photonic crystal (PhC) fibers [9], microrings [6,10] and PhC cavities [11–19]. The smallest possible sensors are the ones based on PhC cavities as their size is of the order of the wavelength, determined by the diffraction limit. Silicon based PhC microcavities have been used to detect (bio) chemical complexes [12–14,19]. Sensors based on III-V semiconductors have been demonstrated as well [11,15,17]. These latter sensors are attractive as they potentially offer the full on-chip integration with sources and detectors, or may be operated as lasers [15] to decrease the detection level. In addition, they can be employed using remote readout, not requiring the delicate attachment of optical fibers or electrical wiring. The principle of array operation for multiplexed sensing was recently shown both for the Si [16] as well as for the InGaAsP III-V system [15].

#122028 - $15.00 USD Received 4 Jan 2010; revised 1 Feb 2010; accepted 1 Feb 2010; published 16 Feb 2010

In this work, we experimentally investigate two different designs of InAs quantum dot-embedded PhC membrane nanocavities for sensing applications using the photoluminescence (PL) technique. The frequency of each mode is tuned across the PhC bandgap by lithographically varying the parameters of many cavities. The systematic increase of the sensitivity of the dipole mode with decrease of the size of the cavity is demonstrated. For a given mode, the sensitivity smoothly increases when the resonance frequency increases towards the upper band edge of the PhC bandgap, irrespective of the detailed design details. Furthermore, the inverse correlation between sensitivity and Quality Factor *Q* is observed.

2. Sample preparation and experimental setup

A 220 nm thick InGaAsP quaternary layer (band edge wavelength 1.25 μm) was grown lattice-matched on a 1 μm InP buffer layer by using Metal-Organic Chemical Vapor Deposition. Rather than the Quantum Wells normally used for photoluminescence in this semiconductor [11,15], here one monolayer of InAs Quantum Dots (density $3x10^{10}$ cm^{-2}) was grown in this layer to generate emission at 1.55 μm wavelength [20]. A 400 nm SiN_x mask was deposited by Plasma Enhanced Chemical Vapor Deposition on a 20 nm InP protective capping layer which was on top of the quaternary layer. The hexagonal pattern of the PhC with the nominal radius-to-lattice spacing (*r/a*) of 0.30 was defined in ZEP 520 resist using Electron Beam Lithography. The SiN_x mask was etched by using Reactive Ion Etching with CHF_3 chemistry. Then the pattern was transferred into the InP-InGaAsP-InP layer stack by Inductively Coupled Plasma etching (ICP) with $Cl_2/Ar/H_2$ chemistry. The final step is the selective wet chemical etching of InP using $HCl:H_2O$ = 4:1 solution at 2 °C to obtain the InGaAsP membrane. Two different cavity types were fabricated, based on defects with no hole missing (H0) [15] and one air hole missing (H1) [21]. These cavities are chosen because they support different types of modes (monopole, dipole etc.), which is useful for comparison. In addition, the same type of mode (e.g. dipole) occurs in both cavity types. Their symmetry and compactness is suitable for integration in an array. Finally, they emit at large out-of-plane angles, which is suitable for the PL-collection. For H0 type of cavities, independent modifications were made on the two adjacent holes in the ΓK-direction (*x*) and/or in the ΓM-direction (*y*) [15]. To distinguish different H0 cavities, they are represented by r_x', s_x, r_y' and s_y as sketched in Fig. 1(a). The six inner holes of the H1 defect cavities were reduced in radius (labeled by r') and/or had their center position shifted radially outward (labeled by s). For a given cavity type, the parameter sets (r_i', s_i) were varied to tune the resonant wavelength for each mode within the bandgap. Figures 1(b) and 1(c) show the Scanning Electron Microscope images of the fabricated H0 and H1 cavities. Due to the fabrication tolerances, the fabricated nanocavities have *r/a* ratio of 0.32 instead of the intended 0.30, as determined from the SEM images.

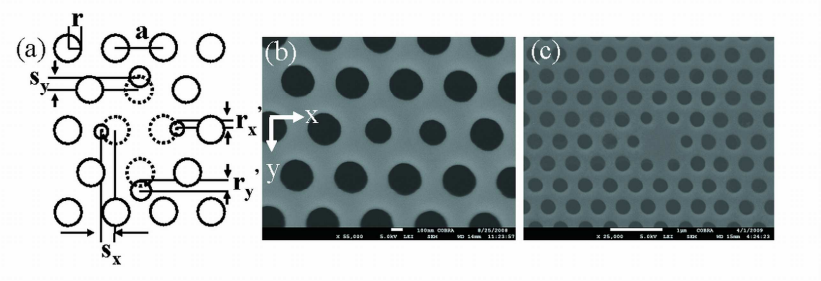

Fig. 1. (a) Schematic of hole modifications; SEM images of fabricated (b) H0(r_x',s_x;r_y',s_y), and (c) H1(r',s) type of InGaAsP nanocavities. The fabricated structure has *r/a* of 0.32.

The cavities were treated by an O_2 plasma and H_3PO_4 etch, which improved the hydrophilicity of the surface. A large, macroscopic, (~1 mm diameter) drop of sugar

#122028 - $15.00 USD Received 4 Jan 2010; revised 1 Feb 2010; accepted 1 Feb 2010; published 16 Feb 2010

(sucrose)-water mixture was placed on the top of the sample from a pipette. This entirely immerses all part of the sample where the cavities are, with the liquid. Then a 0.15 mm thick cover glass was placed on the filled sample in order to avoid water evaporation and to achieve a flat and constant thickness layer of water on top of the sample. This method likely has different infiltration characteristics as compared to the recently developed microinfiltration techniques [22–24]. Since excess fluid is present, not only the holes, but also the top of the sample and under-etched void may be filled with the liquid. The microinfiltration is likely to fill only the holes [24]. A CW diode laser (λ = 660 nm) with a low pump power of 30 μW in order to avoid heating effects is used to excite the cavities. Excitation of the cavities and the collection of the photoluminescence (PL) signals were done by the same 50x microscope objective (N.A. = 0.5). The collected signal was dispersed in a 50 cm monochromator and detected by a liquid nitrogen cooled InGaAs detectors array. The cavity quality factor of the used cavities varied from one to a few times 10^3.

3. Sensitivity determination

Different concentrations of sugar-water solutions with known refractive indices [25] have been infiltrated into the two types of InGaAsP PhC nanocavities in order to investigate the sensitivity of the cavities. After each infiltration, the cavities were cleaned and characterized by PL again. No frequency shifts were detected after the cleaning compared to the unfilled cavity. Figure 2(a) shows the typical spectral response of an H1(r',s), having a nominal lattice spacing of 480 nm with nominal values of r' = 105 nm, and s = 15 nm, to seven different sugar-water concentrations. The resonance peak at 1475 nm (a/λ = 0.34) was identified as a hexapole mode by using 3D finite difference time domain (FDTD) calculations (CrystalWave). After pure water is infiltrated, the hexapole mode redshifts more than 70 nm due to the increase in the ambient refractive index from 1 to 1.33. As the sugar concentration increases, the cavity mode redshifts further. From the slope of the best fit near n = 1.33, the sensitivity, $S = \Delta\lambda/\Delta n$, is determined. For this particular cavity, the sensitivity is 280nm/RIU (refractive index unit). Incomplete filling of the small PhC holes with the analyte is frequently reported [17,19]. The sensitivity depends on how effective the analyte is infiltrated into the holes and the region underneath the holes. This filling is determined by the wetting and governed by capillary forces inside the holes. Therefore, we simulated three different conditions: (1) total filling, (2) surface coverage and filling of the holes, and (3) surface coverage only, by using 3D FDTD. Figure 2(b) shows the 3D FDTD simulation results of the resonant wavelength shift dependence on the refractive index change for three different liquid infiltration conditions as shown in the inset. Sensitivities of 75 nm/RIU, 230 nm/RIU and 285 nm/RIU have been obtained for the surface coverage, surface coverage and hole filling and total filling respectively. Absolute values of calculated and measured resonant wavelengths differ typically by 3% and are caused by fabrication tolerances in the unmodified and modified holes sizes in the cavity. Our experimental result is in good agreement with the calculation; it shows that with a proper treatment of the surface to make it hydrophilic, both the holes in the membrane and the area underneath the membrane can be completely filled. Incomplete, or solution-dependent filling may lead to unpredictable effective sensitivities [17,19].

#122028 - $15.00 USD Received 4 Jan 2010; revised 1 Feb 2010; accepted 1 Feb 2010; published 16 Feb 2010

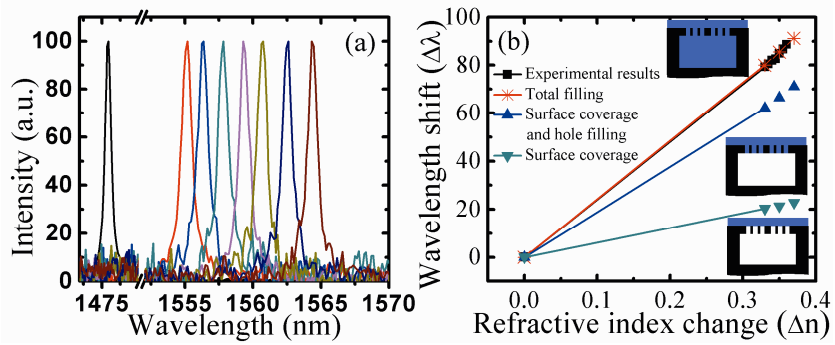

Fig. 2. (a) Resonant wavelength change of an H1(r',s) cavity as the sugar concentration in the sugar-water solution increases. (b) 3D FDTD simulation result for the three different infiltration configurations as represented by the sketches: (i) total filling, (ii) surface coverage and hole filling, and (iii) surface coverage of the sugar-water solutions.

4. Sensitivity dependence on mode frequency

The relation between the sensitivity of a given mode and its position inside the bandgap was investigated. This position was varied by variations in the (r',s) parameters. Figures 3(a) and 3(b) show the sensitivity of the dipole and the monopole modes respectively, obtained from different H0(r_x',s_x;r_y',s_y) cavities as a function of the normalized mode frequency (a/λ) for the cavities in PhC's with three different lattice spacings, 480, 499, 511 nm. Also indicated in the figure are the PhC dielectric band edge near $a/\lambda = 0.29$ and the air band edge near $a/\lambda = 0.37$, as calculated from a 3D FDTD calculation with the experimental membrane parameters with $r/a = 0.32$. The sensitivities increase when the cavity modes are lithographically tuned from the dielectric band to the air band. The same trend has been also obtained for the H1(r',0) type of cavities as follows from Fig. 3(c), which shows that the sensitivity of all supported cavity modes, the dipole (D), the hexapole (H) and the split quadrupole (Q_1 and Q_2) increases when the resonance gets closer to the air band edge. Qualitatively, this behavior is expected since the closer the cavity mode frequencies to the air band edge, the larger the mode overlap with the holes, and thus the higher the sensitivity [26]. The smooth behavior in Fig. 3 suggests that the position within the bandgap mainly determines the sensitivity, irrespective of the details of the cavity design, i.e. in our case the (r',s) sets. The data in Fig. 3 are obtained from measurements with and without water, so that the wavelength shifts are large. Therefore there are no data near the dielectric band edge as these resonances would fall inside the dielectric band after infiltration. From Fig. 3(c) there are data even at or slightly above the air band edge. This is believed to be a real effect as some (rather broad) resonances exist above the band edge, but in the frequency interval between the stopbands in the ΓM and ΓK directions.

#122028 - $15.00 USD Received 4 Jan 2010; revised 1 Feb 2010; accepted 1 Feb 2010; published 16 Feb 2010

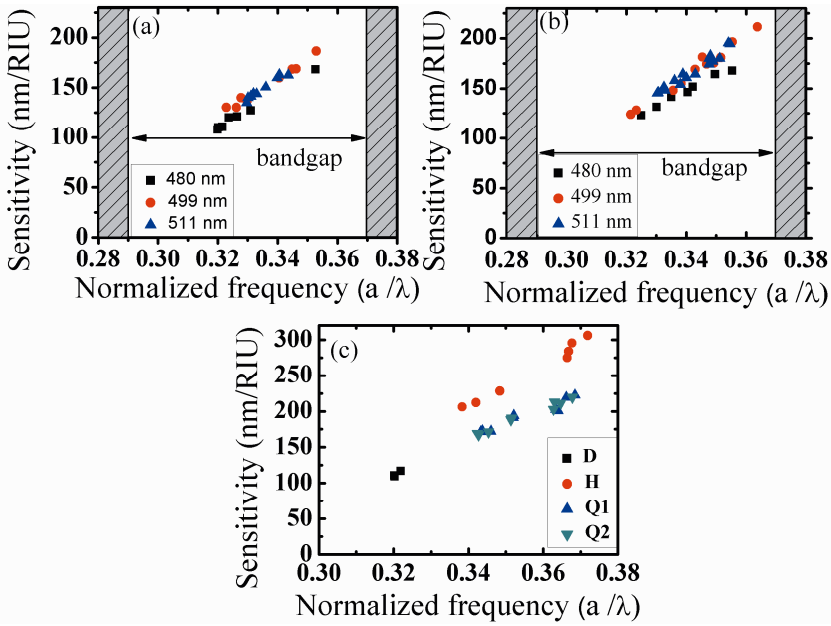

Fig. 3. The sensitivity dependence on the modes' position in the bandgap before infiltration for (a) dipole and (b) monopole mode in H0(r_x',s_x; r_y',s_y) and (c) all cavity modes of H1(r',0) cavities.

A detection limit, which is defined as the minimum detectable refractive index change [27], is the relevant factor for a sensor. For a low detection limit, a high sensitivity and a narrow linewidth i.e. a high *Q* factor are required. A high sensitivity requires a high overlap of the mode profile with the holes, which generally will cause higher losses and a reduction of the *Q* factor. The proper Figure of Merit for a sensor is therefore $S \times Q$ [26], which product should be maximized. Therefore, we experimentally investigated the correlation between the sensitivity and the *Q* factor. Figure 4(a) shows the PL signal collected from an unfilled H0(r_x', s_x; r_y',s_y) cavity where a = 511nm, $r_x' = r_y' = 0.2a$, $s_x = 0.14a$ and $s_y = 0.1a$. The M1 (λ = 1396 nm) and the M2 (λ = 1469 nm) are the higher order modes; the M3 (λ = 1546 nm) and the M4 (λ = 1582 nm) are dipole and monopole modes [15]. Figure 4(b) shows the measured quality factor plotted against the sensitivity for the four modes of the H0 cavity for varying (r_x', s_x; r_y',s_y) parameters. Although there is no clear functional dependence, the expected inverse correlation between S and Q is clearly present [26]. The high Q modes (M3 and M4) are strongly confined inside the dielectric material and have lower sensitivity, whereas the low Q modes (M1 and M2) are less confined inside the dielectric and have a higher sensitivity. The figure suggests that for sensitivities near ~150 nm/RIU the *Q*-factor can be made very large.

#122028 - $15.00 USD Received 4 Jan 2010; revised 1 Feb 2010; accepted 1 Feb 2010; published 16 Feb 2010

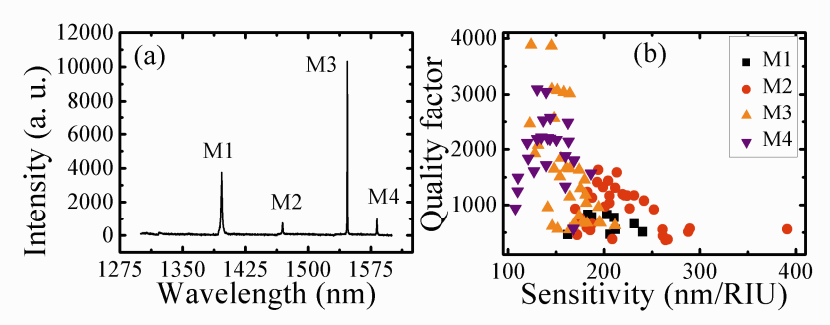

Fig. 4. (a) PL spectrum collected form an H0(r_x', s_x; r_y',s_y) cavity (b) sensitivity correlation with Q factor of the all modes from all H0 type of cavities.

5. Sensitivity dependence on mode and cavity type

Since sensitivities depend on the position of the mode resonance inside the bandgap, it is not straightforward how to compare sensitivities of different cavity-types. For each cavity-type and mode, we have taken the sensitivity as averaged for many H1(r',s) and H0(r_x', s_x; r_y',s_y) configurations, at least ten per cavity-mode type, with frequencies somewhat uniformly spread over the bandgap as in Fig. 3. The results are collected in Table 1. Although the precise values may be arbitrary, as they depend on the exact cavities taken for averaging, some clear trends are observed from Table 1. For a specific cavity, e.g. H1(r',0) cavity, the sensitivity is larger for the modes that are more confined to the perimeter of the cavity such as the hexapole and quadrupole modes. These modes have higher electric field overlap with the holes as compared to the modes which are more localized near the center of the cavity inside the dielectric, e.g. the dipole. The sensitivity of a specific type of mode varies in a characteristic manner with the cavity type. The sensitivity of the dipole increases if the cavity size is reduced by modifying the surrounding holes, which corresponds to going from bottom to top in the table. On the other hand, the modes which are confined near the perimeter of the cavity, like the quadrupole and the hexapole modes, do not depend much on cavity size.

As the resonance wavelength is determined by the average refractive index a mode experiences, the wavelength shift is determined by $S = \Delta\lambda/\Delta n = f\lambda/n$ where $0 \le f \le 1$ which is the overlap of the electromagnetic field with the holes. These maximum values for $S = \lambda/n$ are also displayed in Table 1. The ratio of the average sensitivity divided by the maximum S is given in the last column of Table 1. It shows that the sensitivities are within 30% of the maximum value.

To optimize the sensitivity, special designs have been reported to maximize the overlap of the resonant mode with the holes where the analyte is. Loncar *et al*. obtained a sensitivity of 245nm/RIU from InGaAsP PhC membrane cavities having fractional edge dislocations [11], and with a central hole to increase the overlap. Very recently, Falco et al. obtained a theoretical sensitivity of 585 nm/RIU from their slotted double-heterostructure PhC in Si [19]. Their experimental value was even three times higher, but this was attributed to an improved infiltration as the sugar concentration in the sample increased. Dorfner *et al*. compared two type of cavities, L3 (three missing holes in a row) and H1 with a large central hole in Si. The sensitivities were 63 and 155 nm/RIU respectively, with lower (L3) or comparable (H1) cavity *Q*-factors [14]. A sensitivity of 400nm/RIU has been obtained from InGaAsP cavities in a lasing mode, similar to our H0 cavities, by Kita *et al*. [15]. Kim *et al.* demonstrated a sensitivity of 247nm/RIU for a hexapole mode of a modified single air hole missing cavity [28]. They created a deformed hexapole mode cavity by enlarging two air-holes facing each other.

#122028 - $15.00 USD Received 4 Jan 2010; revised 1 Feb 2010; accepted 1 Feb 2010; published 16 Feb 2010

Table 1. Average sensitivities, maximum sensitivities and filling fraction of different mode types with different cavities.

Cavity Type	Mode Type	Average *S* (nm/RIU)	Maximum *S* (nm/RIU)	Filling Fraction
H0(r',0)	Dipole	$3.1\text{x}10^2$	$1.0\text{x}10^3$	0.30
	Monopole	$2.6\text{x}10^2$	$1.1\text{x}10^3$	0.24
H0(r_x',s_x;r_y',sy)	Second order monopole	$2.0\text{x}10^2$	$1.04\text{x}10^3$	0.20
	Second order dipole	$2.2\text{x}10^2$	$1.15\text{x}10^3$	0.21
	Monopole	$1.6\text{x}10^2$	$1.10\text{x}10^3$	0.15
	Dipole	$1.4\text{x}10^2$	$1.12\text{x}10^3$	0.13
H1(r',0)	Dipole	$1.1\text{x}10^2$	$1.12\text{x}10^3$	0.10
	Hexapole	$2.6\text{x}10^2$	$1.09\text{x}10^3$	0.24
	Quadrupole	$1.9\text{x}10^2$	$1.09\text{x}10^3$	0.18
H1(r',s)	Dipole	$0.9\text{x}10^2$	$1.06\text{x}10^3$	0.08
	Hexapole	$2.8\text{x}10^2$	$1.07\text{x}10^3$	0.27
	Quadrupole	$1.9\text{x}10^2$	$1.08\text{x}10^3$	0.18

6. Conclusion

In this work we reported sensitivities of InAs QDs embedded InGaAsP photonic crystal membrane nanocavities. The sensitivities were determined by infiltrating different concentration of sugar-water solutions inside the holes. 3D FDTD simulation results confirm that the cavities were totally infiltrated. We demonstrated that the sensitivity has a simple relation to the cavity type and increases gradually when the mode frequency increases. The modes which are localized to the periphery of the cavity are found to be more sensitive than the modes localized center of the cavity. We also showed that the sensitivity inversely correlates with the quality factor. Maximum sensitivity of ~300nm/RIU is observed which corresponds to ~25% electric field overlap with the holes. The present experimental data provide insight in the operation of PhC sensors and support theoretical expectations.

Acknowledgement

The authors thank P. A. M. Nouwens, B. Smalbrugge, E. J. Geluk, P. J. van Veldhoven, and T. de Vries for their help in the fabrication processes.

#122028 - $15.00 USD Received 4 Jan 2010; revised 1 Feb 2010; accepted 1 Feb 2010; published 16 Feb 2010